Response Surface Modeling of the Removal of Methyl Orange Dye from an Aqueous Solution Using Magnesium Oxide Nanoparticles Immobilized on Chitosan

Myneni, Venkata Ratnam*[+•]

Department of Chemical Engineering, Mettu University, ETHIOPIA

Kanidarapu, Nagamalleswara Rao

Centre for Disaster Mitigation and Management, Vellore Institute of Technology, Vellore, TamilNadu-632014, INDIA

Shaik, Feroz

Department of Mechanical Engineering, Prince Mohammed Bin Fahd University, Kingdom of SAUDI ARABIA

Vanalapati, Meena

Department of Chemical Engineering, Andhra University, Vizag, INDIA

ABSTRACT: *In this work, the chitosan-based magnesium oxide nanoparticles (CS-MgONP) composite was used as an adsorbent for the removal of the organic dye Methyl Orange (MO). The adsorbent characterization was carried out using X-Ray Diffraction (XRD), Field Emission Scanning Electron Microscopy (FE-SEM), and Fourier Transform InfraRed (FT-IR) spectroscopy. The faster equilibrium, i.e. at an agitation time of 30 min, indicated the faster adsorption capability of the prepared adsorbent CS-MgONP. The Central Composite Design (CCD) of response surface methodology (RSM) was used to evaluate the impact of process parameters in the range of pH (6-10), CS-MgONP dosage (0.1-0.5g/L), MO concentration (10-30mg/L), and temperature (283-323K) at an optimal agitation period of 30 min. Under optimum conditions of pH=7.93, CS-MgONP dosage=0.4g/L, initial MO concentration=15mg/L, and temperature=313 K, 96.42% removal of MO was achieved with desirability of 0.805. The adsorption of MO onto CS-MgONP was best fitted with the Langmuir adsorption isotherm, with an uptake capacity of 237.5 mg/g, and followed the pseudo-second-order kinetics. The thermodynamic studies showed positive enthalpy and negative Gibbs free energy that confirmed the spontaneous and endothermic process. Due to the fast equilibrium agitation period, i.e.30 min, and high adsorption capacity, the adsorbent CS-MgONP proved to be an excellent choice for dye removal.*

KEYWORDS: *Magnesium oxide nanoparticles; Chitosan; Nano-adsorbents; Methyl Orange; RSM; Kinetics; Equilibrium.*

***** *To whom correspondence should be addressed.*

+ *E-mail: mvratnam81@gmail.com*

● *Other Address: Department of Chemical Engineering, Andhra University, Vizag, INDIA*

1021-9986/2022/5/1602-1618 17/$/6.07

INTRODUCTION

Many key sectors, including fabric, pulp, and paper use dyes extensively and dump raw sewage into the surrounding water bodies[1]. Since commercial dyes were biologically non-degradable, the direct discharge of colored effluent water into the aquatic environment decreases the penetration of sunlight and consequently affects the photosynthesis mechanism of aquatic plants [2]. The complex organic molecular structure of dyes makes their removal process harder. Dye disposal was therefore a significant and challenging task in the treatment of wastewater [3]. Many preferred methods of removing synthetic colors from wastewater such as flocculation[4, 5], adsorption [6, 7], photocatalytic degradation[8–13], and oxidation[14] have been implemented. Some of these approaches have disadvantages like inefficiency, high operational costs, secondary pollutant generation, and time-consuming [7].

Among the applicable methods, adsorption realistically was the most efficient technique for the potential removal of color due to its operational effectiveness and simplicity, reasonable cost, and insensitivity to noxious materials[15]. A large amount of literature reports dyes adsorption on various adsorbent surfaces such as activated carbon, chitosan, silica, zeolites, clay, etc. Chitosan was a common biopolymer of nature, widely used in food, pharmaceutical, medical, and environmental products. Chitosan proved as an efficient, low-cost, non-toxic adsorbent[16]. The functional units of amino and hydroxyl groups on the chitosan surface were responsible for its greater adsorption capacity in wastewater treatment[17]. Several published works have been reported in the academic literature with chitosan and its functional derivatives, and chitosan composites as potential sorbents for pollutant removal [18–23]. The adsorption behavior of anionic dyes, eosin Y, and indigo carmine from dilute solution on chitosan was investigated. The experimental data were used to develop a new four-parameter model for correlating liquid-phase adsorption isotherm based on the solid-liquid phase equilibrium [24]. Tweezer-like adsorbents with the enhanced surface area were synthesized by grafting aniline onto the amine sites of a chitosan biopolymer scaffold. Equilibrium solvent swelling results of the adsorbent materials provided evidence of a more polar biopolymer surface upon grafting. Equilibrium uptake studies with fluorescein at ambient pH in aqueous media revealed a high monolayer adsorption capacity of *61.8 mg/g* [25].

In the recent past, much attention has been devoted to nanotechnology. Several articles have mentioned the application of numerous nanoparticles for the treatment and remediation of pollutants [26]. Magnesium oxide nanoparticles (MgONP) are known for their destructive nature toward pollutants, superior adsorption capability, non-toxicity, and moderate cost [27–32]. In addition, because of its favorable electrostatic attractive mechanism, (the pH of the zero point of charge of MgO is 12.4), it is an effective adsorbent for anions [33]. The visible presence of polyhedral defects in synthesized MgONP provides robust surface activity, which led to high adsorption capacity [34]. Several academic researchers synthesized different structured nano-sized magnesium oxides for testing against dye removal. All the studies reported high adsorption capabilities of MgONP along with rapid adsorption rates. In the majority of the cases, it was observed that equilibrium has been attained within 5-30 min of contact time, and hence MgONP is considered a desirable adsorbent for the treatment of dye in wastewater [34-36].

Even though MgONP exhibits excellent adsorption characteristics, the long-term stability of the nanoparticles still stays unanswered. The adsorption capacities and the feasible removal rates will be substantially boosted by possible modification and impregnation techniques. Hence developing nanometal oxide composites will endure a suitable idea. Nanocomposites with chitosan as the matrix phase exhibit excellent adsorption capabilities. *Dehagi et.al* [20] synthesized chitosan–ZnO nanoparticles, which have an excellent adsorption performance towards the successful removal of pesticides with optimum regeneration. *Li et al.* [35] showed that the metal oxide content had a profound effect on the mechanical properties of the synthesized CS/Metal Oxide composite, while carefully studying the CS/Zn composites of appreciably varying weight ratios. *Travlou et al.* [27] functionalized graphite oxide(GO) with magnetic chitosan, which exhibits a higher adsorption capacity of *425mg/g* towards the adsorption of reactive black. *Haldorai et al.* [36] synthesized magnesium nanoparticles immobilized with chitosan. The synthesized composite exhibits good dye (MO) removal along with antibacterial properties.

MgONP was synthesized using clove i.e. *Syzygium aromaticum* extract and tested for the removal of Methylene Blue (MB) and lead ion sensing in an aqueous solution. Maximum 90% MB removal was achieved with an adsorption capacity *of 5555 mg/g*. MgONP was also able to selectively detect lead ions and hence these nanoparticles are useful for dye removal and metal ion sensing applications. MgONP was synthesized by hydrothermal process and tested for the removal of Orange G dye from aqueous solutions. The experimental data followed the pseudo-second kinetic model and was the best fit for Langmuir isotherms [46]. A simple solid-state chemical route has been used to prepare MgONP with a large specific surface area of 213 m^2/g without using liquid solvents, template agents, or surfactants. These nanoparticles showed a superior adsorption capacity of 2375 mg/g towards Congo red. the adsorption behavior obeyed a pseudo-second-order rate equation and the Langmuir isotherm adsorption model [47].

Methyl orange (MO) was a well-known anionic dye, which has been widely used in the textile, printing industries, and research laboratories and has a detrimental impact on living species [37,38]. In this present work, MgONP and chitosan were combined to synthesize a hybrid composite by a simple chemical precipitation method. The synthesized adsorbent was characterized using various analytical instruments and tested for its adsorption capability against methyl orange dye. The key parameters of the adsorption process such as contact time, the dosage of CS-MgO, initial concentration of methyl orange dye, the pH of the dye solution, and operating temperature have been investigated and optimized using Central Composite Design (CCD) of response surface methodology. The kinetic, equilibrium, and thermodynamic studies were carried out for the proper understanding of the adsorption mechanism.

EXPERIMENTAL SECTION

Chemicals and reagents

Magnesium nitrate GR (Mg $(NO_3)_2.6H_2O$) was obtained from Merck Chemicals. Chitosan with a high degree of acetylation (>86 %), polyvinylpyrrolidone (PVP), and ammonium hydroxide (NH_4OH) was purchased from Loba Chemie Pvt. Ltd. Glacial acetic acid, NaOH was procured from Fisher Scientific. Double distilled water was used to prepare all the solutions. P^H adjustments were made by adding 0.1*N* HCl or 0.1*N* NaOH.

Synthesis of adsorbent

Chemical precipitation of 0.5M $Mg(NO_3)_26H_2O$ using PVP as a precipitating agent and ammonium hydroxide as a stabilizer produces MgONP. The Synthesis method employed in this study was adopted from *Haldorai et.al* [36]. The detailed procedure for preparing MgONP was specified precisely in the supplementary information. In a 50 mL one percent (v/v) acetic acid solution, one gram of chitosan flakes was dissolved and stirred at 50°*C* and 500 rpm until a clear solution was obtained. To this, 1 *g* of MgO nanoparticles dispersed in 50 *mL* of one percent (*v/v*) acetic acid solution was added. The solution was constantly stirred until a distinct homogeneous solution was attained. 0.1 *N* NaOH was then added dropwise until pH 10 was reached by the solution. The resulting precipitate was heated for 5 *h* at 80^0C. The solution was rinsed and filtered extensively with distilled water to remove any residual NaOH and dried overnight at 60^0C. The synthesized composite is labeled as CS-MgONP and then used in adsorption experiments.

Characterization of adsorbent

Field emission scanning electron microscopy (FE-SEM Carl Zeiss NTS GmbH, Germany) was used for the study of the size and morphology of synthesized MgONP and CS-MgONP by following standard sample preparation and analysis procedure at an accelerating voltage of 5kV. The studies of X-ray diffraction were performed using Regaku X-ray diffractometer. In the 2θ range of 10-80 degrees, Cu-Kα radiation (λ=1.5418 Aº) was used with a scan rate of 0.05º s^{-1}. The unused and used adsorbent samples FT-IR spectra were recorded using the 4000-400 cm^{-1} Bruker alpha FT-IR spectrometer.

Experimentation and statistical analysis

For adsorption tests, *50mL* of an aqueous solution (containing a specified initial MO dye concentration) was carefully drawn in a 250 mL conical flask. A calculated amount of CS-MgO was added to the aqueous solution and kept on the orbital shaker agitation at room temperature (303*K*). Similarly, in separate conical flasks, more samples with different parameters were prepared. The samples were filtered individually by Whatman grade 42 filter paper after adsorption and evaluated in UV-absorption spectra (wavelength 464 nm) for remaining dye levels.

Table 1: Levels of process variables in coded and un-coded form for % adsorption of MO onto CS-MgONP.

Variable	Name of the Process Variable	Range and levels				
		-2	-1	0	1	2
X_1	pH of the aqueous solution	6	7	8	9	10
X_2	Adsorbent dosage, w, g/L	0.1	0.2	0.3	0.4	0.5
X_3	The initial concentration of MOin aqueous solution, C_o, mg/L	10	15	20	25	30
X_4	Temperature, T, K	283	293	303	313	323

The analysis was repeated thrice to check the reproducibility of the data. The proportion of color adsorption was calculated as $(C_0\text{-}C_e)\ x100/C_0$ where C_0 is the initial MO concentration in an aqueous solution and C_e is the equilibrium concentration of MO in an aqueous solution.

The objective of using RSM was to optimize the process variables simultaneously to achieve the best system performance [39-43]. The three necessary steps in the optimization process: properly conducting the statistically designed experiments, accurately estimating the mathematical model coefficients, and predicting the response, and finally checking the model's adequacy. To optimize process parameters in adsorption studies, CCD can be applied with enormous confidence. The full CCD primarily consists of (1) a complete $2n$ factorial design, where n is the number of test variables, (2) n_0 center points ($n_0 \geq 1$), and (3) two axial points on the axis of each design variable at a distance of $2n/4$ from the design center. Hence, the total number of design points, $N = 2n + 2n + n_0$ and the five levels of the variables were ($-2n/4, -1, 0, +1, +2n/4$). In the current study, a four-factor CCD (central composite design) based on 30 experimental runs on various numerical values of $pH(X_1)$, adsorbent dosage(X_2), initial concentration of dye solution(X_3), Temperature(X_4) was conducted. The main interaction and their contributions to the removal of MO, while keeping the agitation time constant at 30 min were carefully investigated. The lowest ($-\alpha$), low (-1), center-point (0), high ($+1$), and highest ($+\alpha$) levels of each variable considered for the study were tabulated in Table 1.

RESULTS & DISCUSSION

Characterization of adsorbent

The presence of functional groups in the synthesized MgONP, CS-MgO untreated and treated were studied using FT-IR spectroscopic analysis (Fig.1). The formation

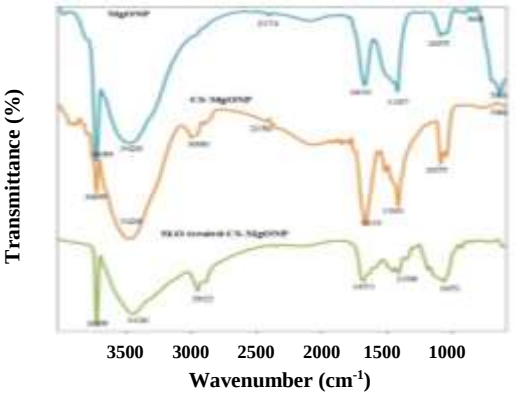

Fig. 1: FT-IR spectra of MgONP, CS-MgONP, and MO-treated CS-MgONP.

of MgONP was amply confirmed by the peak below 500 i.e. at 563 cm^{-1}[44–47]. The peak at 868 cm^{-1} showed the presence of MgO along with δ (O-C=O) due to the usage of magnesium nitrate as the precursor[44]. The presence of peaks at wave numbers 1633, 1387, and 1055 cm^{-1} were typically attributed to carbonate species[44]. Among these, the band at 1055 cm^{-1} was due to C-O-C stretching, 1387 cm^{-1} might be due to the C-OH stretching and 1633 cm^{-1} might be due to C=C stretching. The weak absorption band at 2374 cm^{-1} was attributed to the stretching vibrations of CO_2 as MgO has the nature of adsorbing carbon dioxide and water molecules from the atmosphere due to its surface basic properties[44]. High intense absorption bands at 3420 cm^{-1} were attributed to OH bending and stretching vibrations correspondingly of physically adsorbed H_2O molecules as well as surface OH groups strongly disturbed by hydrogen bonding. The sharp peak at 3699 cm^{-1} on MgO can be functionally related to the presence of hydroxyl groups. The hydroxyl group comes from the reaction between the surface of MgONP with water vapor in the air.

The FT-IR spectral analysis of untreated adsorbent CS-MgONP exhibits narrow bands at 3643 cm^{-1} and 3699 cm^{-1}

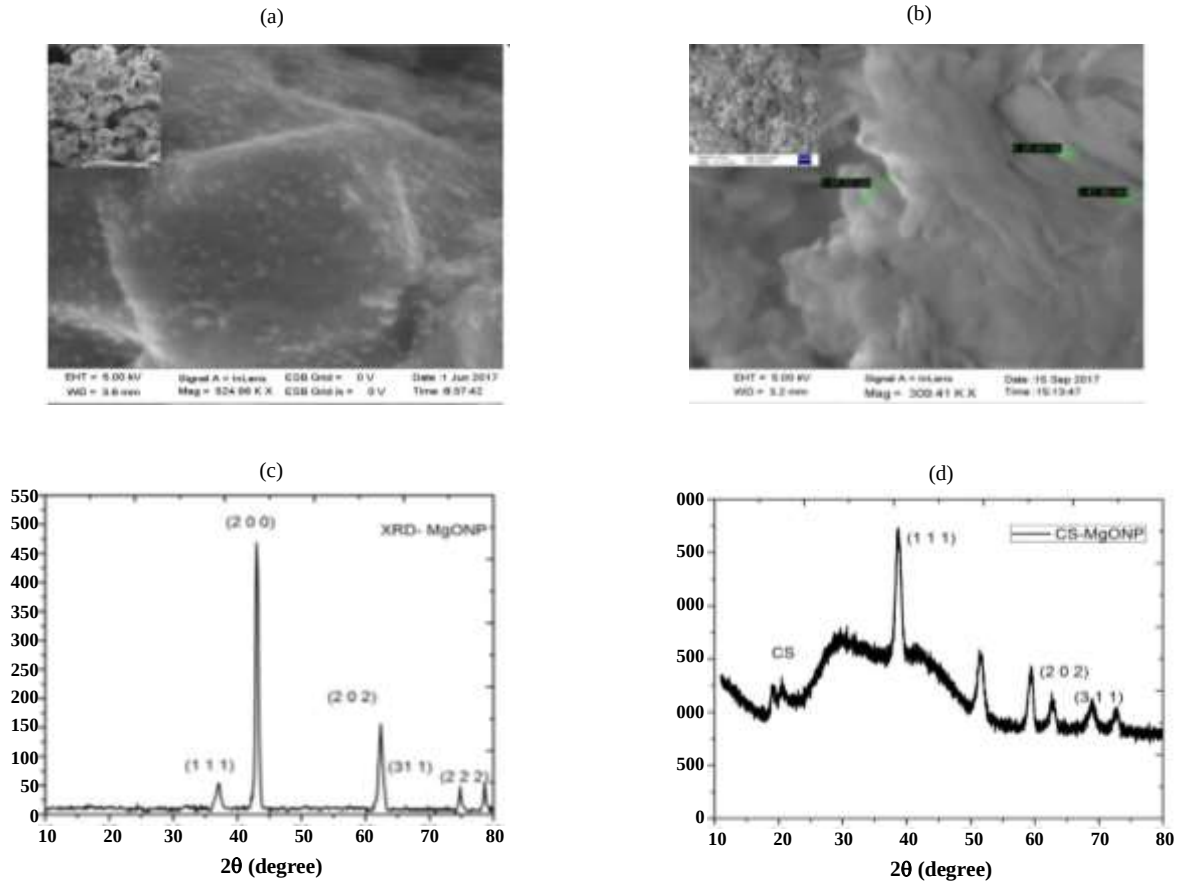

Fig.2: (a) SEM image of MgONP, (b) SEM image of CS-MgONP (c) XRD spectra of MgONP, (d) XRD spectra of CS-MgONP.

due to stretching vibrations correspondingly of physically adsorbed H_2O molecules as well as surface -OH groups, -NH_2 strongly disturbed by hydrogen bonding[48]. The band at 3000 cm^{-1} indicated the presence of stretching C – H vibrations in CH_2 or C = C – H group. The stretch in the band at 1633 cm^{-1}confirmed the presence of the amide group resulting from the compositing of chitosan. In the FT-IR spectra of treated CS-MgONP, aromatic ring vibrations and C-N stretching vibrations, SO_3Na radical vibrations between 1000-1500 cm^{-1}emerge, this reflects the adsorption of MO onto the adsorbent surface. A change in intensities of OH groups at 3695 cm^{-1} was observed in the FT-IR spectra of MO-treated adsorbent, when compared with FTIR spectra of unused adsorbent. Consequently -OH groups could be attributed as one of the prime reason for adsorption, as the OH radicals have the high reaction ability to attack any organic molecule such as SO_3Na. The adsorption of organic dyes occurs by a combination of various mechanisms such as ion exchange, hydrogen bonding, van der walls force, electrostatic attractions, and dipole interactions[49]. In this present study, it seems the electrostatic interactions between adsorbent functional groups and the anionic dye MO played a crucial role in the adsorption process[50].

The FE-SEM image of MgO nanoparticles calcined at 500^0C for 4 hours (Fig.2(a)) showed the assembling morphology of synthesized MgONP particles with a cubic crystal structure. The electron microscopy image (Fig. 2(b)) presented the successful immobilization of MgO onto chitosan. The XRD pattern of the MgONP (Fig. 2(c)) matches well with the cubic crystal system of MgO Periclase phase (JCPDS No: # 96-900-0501). The average crystallite size obtained from the Debby-Scherer equation based on FWHM (full-width-half maximum) calculations for the peak (200) of MgONP was 20.11nm. XRD studies confirmed the preparation of nanoscale materials with a good crystalline structure. Fig. 2 (d) showed the XRD pattern of the magnesium nanoparticles immobilized

chitosan (CS-MgONP). In the synthesized composite, both chitosan, MgO peaks were positively identified. The peak at 20^0adequately reflects chitosan, whereas peaks at 38^0, 62^0 and 74^0reflects the peaks of cubic MgO. The magnesium nanoparticles retain their nanostructure while reinforcing the chitosan matrix. The interaction between chitosan and MgO undoubtedly enhanced the properties of CS–MgO composite. A small amount of hydration of MgO into $Mg(OH)_2$ was evident from other peaks at 50^0 and 58^0[48, 51, 52]

Effect of agitation time

The influence of agitation time on dye removal was investigated using 20mg/LMO solution at pH 5.5, temperature 303 K with an adsorbent dose of 0.2g/L at different agitation times. The results (Fig. S3) indicated that MO was adsorbed instantaneously and that equilibrium was achieved within 30min. The maximum removal of MO was 86.7%. The short equilibrium period indicated precisely the high surface activity of the adsorbent and its suitability to remove dye molecules at a faster rate. The faster equilibrium has occurred because of the availability of active site locations on the adsorbent surface. Further adsorption experiments for the removal of MO were carried out at an equilibrium agitation time of 30min.

Experimental design and optimization using Response Surface Methodology (RSM)

RSM approach will carry out the fitting of mathematical designs to the experimental outcomes produced from the designed experiments. The model confirmation was acquired through statistical methods. The coded and un-coded levels of independent factors, according to 30 experiments, correspond to CCD along with their responses were showed in Table 2.

Regression and the quadratic equation were constructed by means of a CCD to correlate the relationship between approximation and prediction of responses for experimental conditions.

Analysis of variance (ANOVA)

The variance analysis related to the experimental outcomes was provided in *Table 3*. The low probability (< 0.05) of F-value (63.95) suggested the accuracy of the model. The acceptable and reasonable lack of fit with an F value of 0.9955 and probability (> 0.05) showed the method's suitability for excellent experimental data presentation. Significant model terms for response were X_2, X_3, $X4$, X_1X_2, X_1X_3, X_2X_4, and X_3X_4. Consequently, the second-order CCD designs with coded factors were obtained for the process of adsorption:

$$\begin{aligned}\text{Removal of MO} = {} & -90.28827 + 19.66312 \times \text{pH} + \\ & 283.61187 \times \text{dosage}(\text{g/L}) + \\ & 0.51632 \times \text{Concentration}(\text{mg/L}) + \\ & 0.14530 \times \text{Temparature}(^{\circ}\text{K}) + 4.24375 \times \text{pH} \times \text{dosage} + \\ & 0.17813 \times \text{pH} \times \text{Concentration} - \\ & 0.73937 \times \text{dosage} \times \text{Temparature} - 8.66250\text{E} - \\ & 3 \times \text{Concentration} \times \text{Temparature} - 1.51615 \times \text{pH}^2 - \\ & 107.36458 \times \text{dosage}^2 + 0.01275 \times \text{Concentration}^2 + \\ & 7.38542\text{E} - 4 \times \text{Temparature}^2\end{aligned} \quad (1)$$

The positive and negative signs in the above equation (1) reflect the synergistic and antagonistic effects of factors respectively[53]. The model demonstrates a considerably high R^2 value of 0.9783 for MO removal, which indicated that the experimental and predicted results were in good agreement. The predicted R^2 value 0.9562, matches the adjusted R^2 value i.e. 0.9630. From Fig.3 (a), it was demonstrated that the expected model response was consistent with calculated values over the chosen range of independent variables, with high R^2 values. The model's adequate precision (signal-to-noise ratio) of 28.764, indicated an appropriate signal and showed that this model can be used to navigate the design space[48].

Response surface plots and interactions between the adsorption parameters for MO adsorption using CS-MgONP

The contour charts of the percentage adsorption of MO vs. interactive impacts of solution pH, initial concentration of MO, adsorbent dosage, and aqueous solution temperature were shown in Figs. 4 (a)–4 (d). Each contour chart was a combination of two test parameters with the other parameters kept at zero levels. The non-linear nature of all 3D response surfaces indicated significant relationships between the dependent factors and the removal percentage of MO.

Table 2: Results from CCD for MO adsorption onto CS-MgONP.

Run no.	X_1, pH	X_2, w	X_3, C_0	X_4, T	% adsorption of MO	
					Experimental	Predicted
1	-1.000	-1.000	-1.000	-1.000	85.16	85.45
2	1.000	-1.000	-1.000	-1.000	82.56	82.67
3	-1.000	1.000	-1.000	-1.000	92.3	92.29
4	1.000	1.000	-1.000	-1.000	91.16	91.20
5	-1.000	-1.000	1.000	-1.000	83.15	83.19
6	1.000	-1.000	1.000	-1.000	84	83.96
7	-1.000	1.000	1.000	-1.000	89.26	89.26
8	1.000	1.000	1.000	-1.000	91.47	91.73
9	-1.000	-1.000	-1.000	1.000	91.4	91.12
10	1.000	-1.000	-1.000	1.000	89.45	89.61
11	-1.000	1.000	-1.000	1.000	94.8	94.99
12	1.000	1.000	-1.000	1.000	95.24	95.18
13	-1.000	-1.000	1.000	1.000	87	87.12
14	1.000	-1.000	1.000	1.000	89.18	89.17
15	-1.000	1.000	1.000	1.000	90.36	90.23
16	1.000	1.000	1.000	1.000	94.12	93.98
17	-2.000	0.000	0.000	0.000	85.14	85.10
18	2.000	0.000	0.000	0.000	86.15	86.06
19	0.000	-2.000	0.000	0.000	81.65	81.53
20	0.000	2.000	0.000	0.000	93.18	93.17
21	0.000	0.000	-2.000	0.000	94.8	94.65
22	0.000	0.000	2.000	0.000	91.17	91.19
23	0.000	0.000	0.000	-2.000	88.26	87.98
24	0.000	0.000	0.000	2.000	95.75	95.89
25	0.000	0.000	0.000	0.000	90.88	91.64
26	0.000	0.000	0.000	0.000	92.67	91.64
27	0.000	0.000	0.000	0.000	90.27	91.64
28	0.000	0.000	0.000	0.000	91.8	91.64
29	0.000	0.000	0.000	0.000	93.36	91.64
30	0.000	0.000	0.000	0.000	90.88	91.64

Table 3ANOVA Table for model to predict % removal of MO by CS-MgONP using CCD

Source	Sum of Squares	Df	Mean Square	F Value	p-value
Model	442.44	12	36.87	63.95	< 0.0001
X_1-pH	1.39	1	1.39	2.41	0.1393
X_2-dosage	203.41	1	203.41	352.80	< 0.0001
X_3-Conc.	18.01	1	18.01	31.24	< 0.0001
X_4-Temp	93.89	1	93.89	162.85	< 0.0001
X_1X_2	2.88	1	2.88	5.00	0.0391
X_1X_3	12.69	1	12.69	22.01	0.0002
X_2X_4	8.75	1	8.75	15.17	0.0012
X_3X_4	3.00	1	3.00	5.21	0.0357
X_1^2	63.05	1	63.05	109.35	< 0.0001
X_2^2	31.62	1	31.62	54.84	< 0.0001
X_3^2	2.79	1	2.79	4.84	0.0420
X_4^2	0.15	1	0.15	0.26	0.6170
Residual	9.80	17	0.58		
Lack of Fit	2.72	12	0.23	0.16	0.9955
Pure Error	7.08	5	1.42		
Cor Total	452.25	29			

df- degree of freedom; SS- sum of squares; F- factor F; P- probability

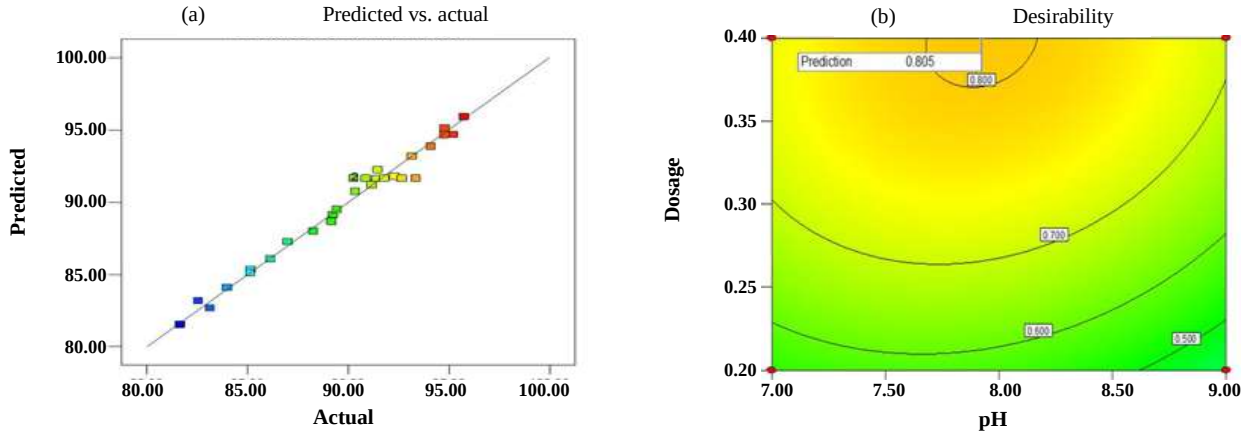

Fig. 3: (a) Comparison plot between the experimental data and predicted data for the adsorption of MO onto CS-MgONP; (b) Desirability plot for MO Adsorption onto CS-MgONP

The combined effect of solution pH (X_1) and CS-MgONP dosage (X_2) was significant (p-value of 0.0391 as obtained in Table 3) on MO removal while keeping the other factors, initial concentration of MO(20mg/L) and solution temperature(303K) constant. Fig.4 (a), showed the 3-D surface plot for the interactive effect of X_1X_2; it is evident that enhancement in CS-MgONP dosage and decrease in the solution pH led to increased removal of MO. At lower dosages, the adsorbent's ability to remove MO decreased because of the higher ratio

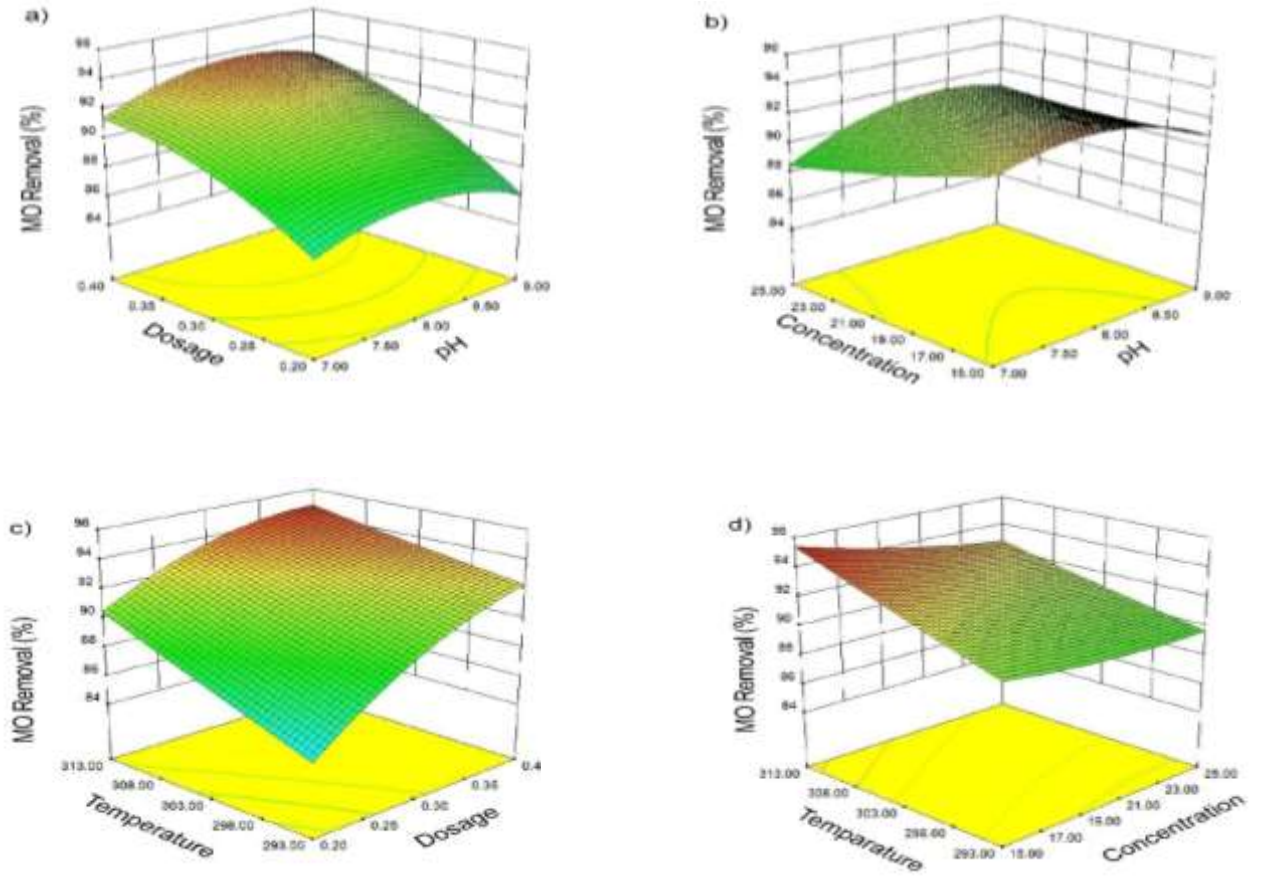

Fig.4: Three-dimensional response surface plots for adsorption of MO onto CS-MgONP: Interactive effects of (a) pH and Dosage (b) pH and Concentration (c) Dosage and Temperature (d) Concentration and Temperature.

on the adsorbent surface between MO molecules and vacant sites[9]. Due to the low ratio of solution concentration to adsorbent sites, the MO removal percentage was good at a lower MO initial concentration. Whereas at higher concentrations, a less adsorption rate was identified because of the saturation of adsorption sites [55]. The simultaneous increase in the dose of adsorbents and solution temperature indicated an improvement in the proportion of MO removal as shown in Fig.4(c). Fig.4 (d) demonstrated an increasing trend with temperature and an adverse trend with initial MO concentration. The increase in percentage MO removal with an increase in temperature up to 313K indicates the endothermic nature of MO adsorption.

Optimization

Fig.3(b) showed the desirability profile for the percent removal of MO vs. the dependent variables. The variation in desirability from 0.0 to 1.0 refers to reaching the very desirable situation from the undesirable. The experiments were conducted in order to evaluate the percentage of adsorption of MO and the results were tallied by the percentage of MO removal achieved through desirability assessment.

Adsorption Kinetic Study

The efficient design of the adsorption process undoubtedly requires the analysis of adsorption behavior through kinetic data. One or a combination of pathways such as chemical reaction, diffusion, and mass transfer will affect the process. The kinetics of MO adsorption onto CS-MgONP was properly analyzed with four different models, i.e. pseudo-first-order, pseudo-second-order, Elovich, and intra-particle diffusion kinetic models. The experimental data at various agitation times were recorded for an aqueous solution of MO with 20mg/L concentration at a pH = 8, T= 303 K, and an adsorbent dosage of 0.3g/L. The MO experimental data for kinetics was analyzed using

Table 4 Kinetic parameters and their correlation coefficients calculated for the adsorption of MO onto CS-MgONP(pH=8; dosage= 0.3g/L; Concentration =20mg/L; Temperature=303K)

Model	Parameters	Values (Linear regression)	Values (Non-Linear regression)
Pseudo-First order[56] $q_t = q_e(1 - e^{-k_1 t})$	k_1(min^{-1})	0.08205	0.9255
	q_e (calc) mg/g	20.16	55.37
	R^2	0.9362	0.8161
	χ^2		1.5261
Pseudo-Second order[57] $q_t = \frac{q_e^2 k_2 t}{1 + q_e k_2 t}$	k_2(g/(mg.min)	0.0181	0.0261
	q_e(calc)mg/g	61.46	59.93
	R^2	0.9982	0.9602
	χ^2		0.3058
Elovich [58] $q_t = \frac{\ln(1 + \alpha\beta t)}{\beta}$	β(g/mg)	0.1563	0.1563
	α (mg/g.min)	3374.9	3373.15
	R^2	0.918	0.9285
	χ^2		0.6876
Intra-particle diffusion[59] $q_t = k_{diff} t^{0.5} + C$	K_{diff}(mg/g.$min^{1/2}$)	4.665	4.6650
	C(mg. g-1)	38.558	38.5578
	R_i	0.3623	0.3623
	R^2	0.8006	0.8255
	χ^2		1.6159
	q_e(Exp.)mg/g	62.9	

linear (Fig.S1) and non-linear regression analysis (Fig. 5(a)). To identify the best kinetic and isotherm models that fit the experimental data, the calculation of chi-squared value (χ^2) was recommended in addition to calculating the coefficient of determination R-square (R^2) for the non-linear method. The regression coefficients along with the kinetic constants for both linear and non-linear analyses were presented for the qualitative comparison in Table.4.

The distortion of pseudo-first-order kinetics by linearization was evident from the comparison of q_e values. The direct applicability of pseudo-second-order kinetics for interpretation of experimental data of MO adsorption by CS-MgONP adsorbent was evident in high values and low χ^2 values. Fig. 5(a) showed the suitability of the Elovich model for the representation of kinetics data corresponding to the present adsorption system with R^2=0.92 and χ^2=0.6876. From the Milovich model, it has been identified that the sorption of MO onto CS-MgONP was remarkably fast with a very high initial rate constant (α) of 3373.15 mg/g.min and a low desorption rate constant (β= 0.1563g/mg). For the intra-particle diffusion model shown in Fig. 5(b), the values of q_t showed multi-linearity correlated with values of $t^{1/2}$. The R_i value of 0.3623, which was between 0.1-0.5, indicated the process corresponds to strong initial adsorption, more controlled by the surface layer. The boundary layer thickness was obtained as 38.558 mg/g. The rate constant for intra-particle diffusion (K_{diff}), was estimated at 4.665 mg/g.$min^{1/2}$.

Adsorption isotherms

Isotherm models such as Langmuir, Freundlich, Temkin, and R-P isotherm were used for the fitting of experimental data. This helps in properly designing an effective adsorption process for handling pollutants. The adsorption equilibrium data were fitted with Isotherms in the non-linear regression model. The isotherm constants and regression constants (R^2, χ^2) were tabulated in Table 5.

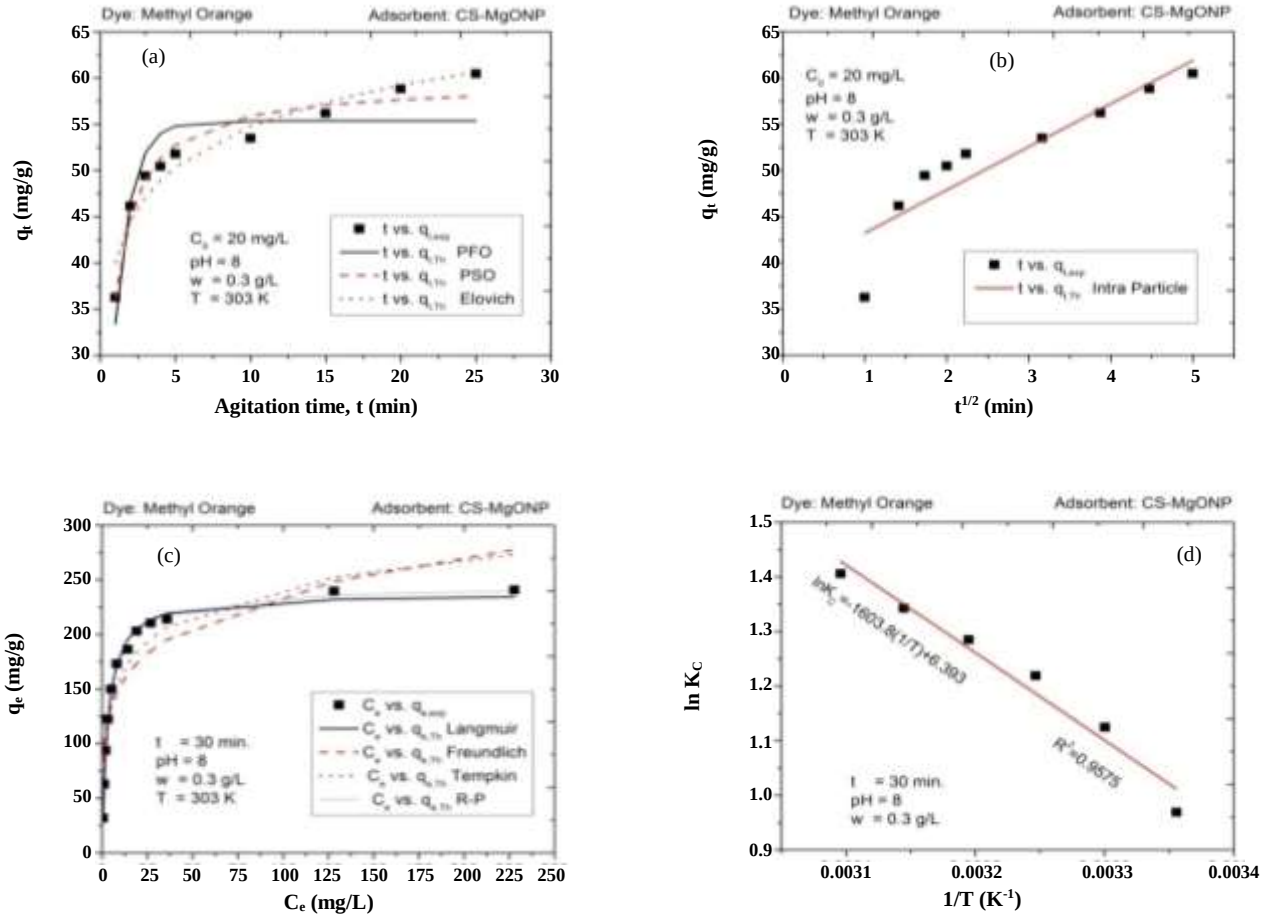

Fig.5: (a) Kinetic models PFO, PSO, and Elovich (b) Intrapraticle Diffusion Model (c) Adsorption Isotherms (d) Thermodynamic Studies of MO adsorption onto CS-MgONP.

In comparison with the isotherm parameters obtained from linear regression, non-linear regression parameters were better at representing the actual experimental values. Three-parameter isotherms such as R-P isotherms were better fitted with non-linear regression rather than the trial and error procedure of fitting employed in linear regression. The Langmuir isotherm, which accurately represents the monolayer adsorption of the adsorbate, fits the experimental data, with a high R^2 value 0.99 (shown in Fig. 5(C)). The high value of adsorption capacity (q_{max}=237.5mg/g), calculated from the slope of the Langmuir equation indicated the adsorption nature of CS-MgONP. The separation factor (R_L) values calculated based on the intercept of the K_L were in the range of 0.01-0.2332, showed that adsorption was favorable. High values of Freundlich constant K_F (L/mg) can be taken as a relative indicator of the high adsorption capacity of CS-MgONP adsorbent and the value of n, another Freundlich constant less than 1 confirmed favorable adsorption. From the adsorption equilibrium data fitted with Temkin isotherm, the heat of adsorption (b) was obtained as 69.763 J/mol with an equilibrium binding capacity of 8.722 L/mg. The constant of R-P isotherm 'g' value, which lies between 0 and 1 (0.9902) indicated that the model was approaching Langmuir Isotherm.

Thermodynamics

For the investigation of the adsorption mechanism, thermodynamic studies of MO adsorption to CS-MgONP were performed. Various thermodynamic constants such as the change in the standard free energy (ΔG°), enthalpy (ΔH°), and entropy (ΔS°) were calculated. The values were tabulated in Table6. The values of ΔH° and ΔS° were given by a graph on ln(K_C) vs 1/T as shown in Fig. 5(d). At every temperature, the values for ΔG° have been discovered negative, showing that the adsorption of MO to

Table 5: Isotherm constants and their correlation coefficients calculated for the adsorption of MO onto CS-MgONP(Agitation time = 30 min., pH=8; dosage= 0.3 g/L; Temperature=303 K).

	parameters	Values (Linear regression)	Values (Non-Linear regression)
	q_{max}(mg/g)	244.5	237.51
	k_L(L/ mg)	0.2759	0.3287
	R_L	0.0019-0.266	0.01-0.2332
	R^2	0.9998	0.9956
	χ^2		1.141
Freundlich [61] $q_e = K_F C_e^n$	n	0.2977	0.1899
	K_F (mg/g)/(mg/L)^n	70.745	98.94
	R^2	0.7833	0.8214
	χ^2		76.186
Temkin[62] $q_e = B \ln(C_e K_T)$	B	36.11	35.96
	K_T(L/mg)	9.002	8.722
	R^2	0.9298	0.9362
	χ^2		24.67
Redlich-Peterson[63] $q_e = \frac{k_{rp} C_e}{(1 + a_{rp} C_e^g)}$	k_{rp} (L/g)	157	80.1
	a_{rp} ((mg/L)$^{-g}$	1.475	0.3478
	g	0.7953	0.9902
	R^2	0.9758	0.9943
	χ^2		0.1853

CS-MgONP was spontaneous. The positive value for ΔH° stated that adsorption was endothermic because a temperature rise improves the propagation frequency of adsorbed molecules across the external boundary layer and the inner pores of adsorbent materials. The positive value of ΔS° indicated enhanced disturbance during sorption on the solid-solution interface.

Mechanism of adsorption

The high surface activity of MgONP and the -OH functional groups present seemed to be the prime reasons for adsorption. For the composite CS-MgONP, the adsorption mechanism was identified through FT-IR analysis. It demonstrated the presence of aromatic ring vibrations and C-N stretching vibrations, SO_3Na radical vibrations, which indicated the attachment of dye molecules onto the adsorbent surface in the case of CS-MgONP. The adsorption might be resulting because of the electrostatic attractions between the anionic dye surface and the positively charged CS-MgONP surface. A comparison of the calculated maximum adsorption capacities (q_{max}) for MO adsorption from the Langmuir equation with q_{max} values of other adsorbents in the literature were presented in Table 7.

CONCLUSIONS

● Equilibrium agitation time for adsorption was obtained as 30min for CS-MgONP. The rapid equilibrium agitation times for the MO removal could be attributed to the positive surface charge of magnesium oxide nanoparticles over a broad range of pH (pH_{ZPC}=11), which showed more attraction towards anionic dyes.

● MO removal % at the optimal variables by CCD-RSM was 96.42% for CS-MgONP.

● The experimental kinetic data followed the pseudo-second-order kinetics & the experimental isotherm data was best fitted with the Langmuir isotherm.

● Non-linear regression proved to be better at fitting the experimental data with the kinetic and isotherm

Table 6: Thermodynamic parameters for adsorption of MO by CS-MgONP.

Temperature (K)	Equilibrium Constant K_C	ΔG^o (K.J/mol)	ΔH^o (J/mol.K)	ΔS^o (J/mol.K)	Van't Hoff Equation
298	2.635	-2.4005	13.334	53.1514	$\ln K_C$= -1603.8(1/T)+6.393 R^2= 0.9575
303	3.079	-2.8330			
308	3.384	-3.1217			
313	3.614	-3.3435			
318	3.829	-3.5497			
323	4.078	-3.7747			

Table 7: Comparison of MO adsorption capacity with other adsorbents.

Adsorbent	Adsorption Capacity (*mg/g*)	Ref.
Hybrid crosslinked chitosan-epichlorohydrin/TiO2 nanocomposite (CTS-ECH/TNC)	210	[7]
crosslinked chitosan-glyoxal and 50 %TiO2 nanocomposite CCG/ TNC-50	416.1	[16]
cross-linked chitosan-glutaraldehyde with 25% nano TiO_2 CS-GLA/TNC-25	103.1	[49]
CNT/C@Fe/chitosan composites	500	[50]
Chitosan/Al_2O_3/magnetic iron N.P	417	[51]
Chitosan/Kaolin/α-Fe_2O_3 nanocomposites	37	[52]
Magnetite/pectin	126.58	[66]
Magnetite silica/pectin	60.61	
Magnetic Chitosan Composite	149.3	[67]
Magnetic chitosan enwrapping nanosized α-Fe_2O_3 and multi-walled carbon nanotubes	66.1	[68]
Chitosan/alumina composite	32.7	[69]
CS-MgONP	237.5	Present Study

models, especially for the pseudo-first-order kinetic model and Redlich-Peterson Isotherm.

● Adsorption mechanism was identified through FT-IR analysis, which revealed the presence of aromatic ring vibrations & C-N stretching vibrations, SO_3Na radical vibrations. This indicated the attachment of dye molecules onto the adsorbent surface in the case of CS-MgONP. The adsorption might be resulting because of the electrostatic attractions between the anionic dye surface and the positively charged CS-MgONP surface.

● The adsorption capacity, which would be considered a vital parameter for evaluating the suitability of the adsorbent was obtained as 237.5*mg/g* for CS-MgONP.

Received : May. 3, 2021 ; Accepted : Aug. 16, 2021

REFERENCES

[1] Hajira T, Atika S, Muhammad S., Synthesis of Kaolin Loaded Ag and Ni Nanocomposites and Their Applicability for the Removal of Malachite Green Oxalate Dye, *Iran. J. Chem. Chem. Eng. (IJCCE)*, **37**: 11–22 (2018).

[2] Kamranifar M, Naghizadeh A., Montmorillonite Nanoparticles in Removal of Textile Dyes from Aqueous Solutions: Study of Kinetics and Thermodynamics, *Iran. J. Chem. Chem. Eng. (IJCCE)*, **36**: 127–137 (2017).

[3] Myneni V.R., Punugoti T., Kala N.S., Kanidarapu N.R., Vangalapati M., Modelling and optimization of Methylene Blue Adsorption onto Magnesium Oxide Nanoparticles Loaded onto Activated Carbon (MgONP-AC): Response Surface Methodology and Artificial Neural Networks, *Mater. Today Proc*, **18**: 4932–4941 (2019).

[4] Gadekar M.R., Ahammed M.M., Coagulation/ Flocculation Process for Dye Removal using Water Treatment Residuals: Modelling Through Artificial Neural Networks, *Desalin Water Treat*., **57**: 26392–26400 (2016).

[5] Wang J., Yao W., Gu P., Yu Sh., Wang X., Du Y., Wang H., Chen Z., Hayat T., Wang X., Efficient Coagulation of Graphene Oxide on Chitosan–Metal Oxide Composites from Aqueous Solutions, *Cellulose*, **24**: 851–861 (2017).

[6] Abbasi S., Adsorption of Dye Organic Pollutant Using Magnetic ZnO Embedded on the Surface of Graphene Oxide, *J Inorg Organomet Polym Mater*., **30**: 1924–1934 (2019).

[7] Jawad A.H., Mubarak N.S.A., Abdulhameed A.S., Hybrid Crosslinked Chitosan-Epichlorohydrin/TiO_2 Nanocomposite for Reactive Red 120 Dye Adsorption: Kinetic, Isotherm, Thermodynamic, and Mechanism Study, *J Polym Environ* **28**: 624–637 (2020).

[8] Fakhrzad M, Navidpour A.H., Tahari M., Abbasi.S., Synthesis of Zn2SnO4 Nanoparticles Used for Photocatalytic Purposes Mater, *Res. Express*, **6**: 095037, (2019).

[9] Fakhrzad M., Navidpour A.H., Tahari M., Abbasi S., Photocatalytic Removal of Methyl Orange in Suspension Containing ZnO and SnO_2 Nanoparticles and Investigation the Influence of Effective Variables on the Process, *Iranian Journal of Health and Environment*, **9(3)**:433-42 (2016)

[10] Ghaderi A., Abbasi S., Farahbod F., Synthesis, Characterization and Photocatalytic Performance of Modified ZnO Nanoparticles with SnO_2 Nanoparticles, *Mater. Res. Express*, **5(6)**: (2018).

[11] Abbasi S, Ahmadpoor F, Imani N, Mehri K., Synthesis of Magnetic Fe_3O_4@ZnO@Graphene Oxide Nanocomposite for Photodegradation of Organic Dye Pollutant, *International Journal of Environmental Analytical Chemistry*, **100(2)**: (2019).

[12] Navidpour AH, Fakhrzad M, Tahari M, Abbasi S., Novel Photocatalytic Coatings Based on Tin Oxide Semiconductor, *Surf. Eng.*, **35**: 216–226 (2019).

[13] Ratnam M.V., Karthikeyan C., Rao K.N., Meena V., Magnesium oxide Nanoparticles for Effective Photocatalytic Degradation of Methyl Red Dye in Aqueous Solutions: Optimization Studies Using Response Surface Methodology, *Mater. Today Proc.* **26(2)**: 2308-2313(2020)

[14] Wang L., Jiang J., Pang S.Y., Zhou Y., Sun Sh., Gao Y., Jiang Ch.G., Oxidation of Bisphenol a by Nonradical Activation of Peroxymonosulfate in the Presence of Amorphous Manganese Dioxide. *Chem. Eng. J.*, **352**: 1004–1013 (2018).

[15] Özer D., Aksu Z., Kutsal T., Çaglar A., Adsorption Isotherms of Lead(ii) and Chromium(vi) on Cladophora Crispata, *Environ Technol (United Kingdom)*, **15**: 439-448 (1994).

[16] Mohammad AKT, Abdulhameed AS, Jawad AH., Box-Behnken Design to Optimize the Synthesis of New Crosslinked Chitosan-Glyoxal/TiO_2 Nanocomposite: Methyl Orange Adsorption and Mechanism Studies, *Int J Biol Macromol* **129**: 98–109 (2019).

[17] Wu FC, Tseng RL, Juang RS., A Review and Experimental Verification of Using Chitosan and Its Derivatives as Adsorbents for Selected Heavy Metals, *J Environ Manage*, **91**: 798–806 (2010).

[18] Fan L, Luo C, Li X, Li X., Lu F., Qiu H., Sun M., Fabrication of Novel Magnetic Chitosan Grafted with Graphene Oxide to Enhance Adsorption Properties for Methyl Blue, *J. Hazard Mater*, **215–216**: 272–279 (2012).

[19] Yang D., Qiu L., Yang Y., Efficient Adsorption of Methyl Orange Using a Modified Chitosan Magnetic Composite Adsorbent, *J. Chem. Eng. Data*., **61**: 3933–3940 (2016).

[20] Moradi Dehaghi S., Rahmanifar B., Moradi A.M., Azar P.A., Removal of Permethrin Pesticide from Water by Chitosan-Zinc Oxide Nanoparticles Composite as an Adsorbent, *J Saudi Chem Soc.*, **18**: 348–355 (2014)

[21] Travlou N.A., Kyzas G.Z., Lazaridis N.K., Deliyanni E.A., Functionalization of Graphite Oxide with Magnetic Chitosan for the Preparation of a Nanocomposite Dye Adsorbent. *Langmui*, **29(5)**: 1657–1668(2013).

[22] Vakili M., Rafatullah M., Salamatinia B., Zuhairi Abdullah A., Hakimilbrahim M., Bing Tang K., Gholami Z., Amouzgar P., Application of Chitosan and its Derivatives as Adsorbents for Dye Removal from Water and Wastewater: A Review, *Carbohydr Polym*, **113**: 115–130 (2014).

[23] Chatterjee S., Chatterjee T., Lim S., Woo S.H., Adsorption of a Cationic Dye, Methylene Blue, on to Chitosan Hydrogel Beads Generated by Anionic Surfactant Gelation, *Environ Technol*., **32**: 1503–1514(2011).

[24] Gopinathan R., Bhowal A., Garlapati C., Adsorption Studies of Some Anionic Dyes Adsorbed by Chitosan and New Four-Parameter Adsorption Isotherm Model, *J. Chem. Eng. Data*, **64(6)**: 2320-2328 (2019).

[25] Vafakish B., Wilson L.D., Surface-Modified Chitosan : An Adsorption Study of a " Tweezer-Like " Biopolymer with Fluorescein, *Surfaces*, **2(3)**: 468-484 (2019).

[26] Hu J., Song Z., Chen L., Yang H., Li J., Richards R., Adsorption Properties of MgO(111) Nanoplates for the Dye Pollutants from Wastewater, *J. Chem. Eng. Data*, **55**: 3742-3748 (2010).

[27] Purwajanti S., Zhou L., Ahmad Nor Y., Zhang J., Zhang H., Huang X., Yu Ch., Synthesis of Magnesium Oxide Hierarchical Microspheres: A Dual-Functional Material for Water Remediation. *ACS Appl. Mater. Interfaces*, **7**: 21278–21286(2015).

[28] Sawai J., Kojima H., Igarashi H., Hashimoto A., Shoji S., Sawaki T., Hakoda A., Kawada E., Kokugan T., Shimizu M., Antibacterial Characteristics of Magnesium Oxide Powder, *World J. Microbiol. Biotechnol.*, **16**: 187–194 (2000).

[29] Cao C.Y., Qu J., Wei F., Li H., Song W.-G., Superb Adsorption Capacity And Mechanism of Flowerlike Magnesium Oxide Nanostructures for Lead and Cadmium Ions, *ACS Appl. Mater. Interfaces* 4:4283–4287(2012).

[30] Kim Y.H., Tuan V.A., Park M.K., Lee C.H., Sulfur Removal from Municipal Gas Using Magnesium Oxides and a Magnesium Oxide/Silicon Dioxide Composite, *Microporous Mesoporous Mater.*, **197**: 299–307(2014).

[31] Dhal J.P., Sethi M., Mishra B.G., Hota G., MgO Nanomaterials with Different Morphologies and Their Sorption Capacity for Removal of Toxic Dyes, *Mater Lett.*, **141**: 267–271(2015)

[32] Soleimani F., Salehi M., Gholizadeh A., Comparison of Visible Light Photocatalytic Degradation of Different Pollutants by (Zn, Mg) x Cu 1-x Bi_2O_4 Nanoparticles, *Ceram Int.*, **45**:8926–8939(2019).

[33] Nga N.K., Hong P.T.T, Lam T.D., Huy T.Q., A Facile Synthesis of Nanostructured Magnesium Oxide Particles for Enhanced Adsorption Performance in Reactive Blue 19 Removal, *J Colloid Interface Sci.*, **398**: 210–216(2013).

[34] Madzokere T.C., Karthigeyan A., Heavy Metal Ion Effluent Discharge Containment Using Magnesium Oxide (MgO) Nanoparticles, *Mater Today Proc.*, **4**: 9-18 (2017).

[35] Li L.H., Deng J.C., Deng H.R., Liu Z.-L., Xin L., Synthesis And Characterization of Chitosan/ZnO Nanoparticle Composite Membranes, *Carbohydr Res.*, **345**: 994-998 (2010).

[36] Haldorai Y., Shim J.J., An Efficient Removal of Methyl Orange Dye from Aqueous Solution by Adsorption onto Chitosan/MgO Composite: A Novel Reusable Adsorbent, *Appl Surf Sci.*, **292**: 447-453 (2014).

[37] Chen S., Zhang J., Zhang C., Yue Q., Li C., Li Y., Equilibrium and Kinetic Studies of Methyl Orange and Methyl Violet Adsorption on Activated Carbon Derived from Phragmites Australis, *Desalination*, **252**: 149–156 (2010).

[38] Abbasi S., Hasanpour M., Variation of the Photocatalytic Performance of Decorated MWCNTs (MWCNTs-ZnO) with pH for Photo Degradation of Methyl Orange, *Journal of Materials Science Materials in Electronics*, **28(2)**: (2017).

[39] Abbasi S., Hasanpour M., Ahmadpoor F., Sillanpää M., Dastan D., Achour A., Application of the Statistical Analysis Methodology for Photodegradation of Methyl Orange Using a New Nanocomposite Containing Modified TiO_2 Semiconductor with SnO_2, *Int J Environ Anal Chem.*, **00**: 1–17 (2019).

[40] Abbasi S., Photocatalytic Activity Study of Coated Anatase-Rutile Titania Nanoparticles with Nanocrystalline Tin Dioxide Based on the Statistical Analysis, *Environ Monit Assess*, **191**: 206(2019).

[41] Abbasi S., Mehri K., Tahari M., Modeling and Predicting the Photodecomposition of Methylene Blue via ZnO–SnO2 Hybrids Using Design of Experiments (DOE), *Journal of Materials Science Materials in Electronics*, **28(3)**: 15306–15312 (2017).

[42] Roozban N., Abbasi S., Ghazizadeh M., The Experimental and Statistical Investigation of the Photo Degradation of Methyl Orange Using Modified MWCNTs with Different Amount of ZnO Nanoparticles, *Journal of Materials Science Materials in Electronics* **28(10)**: 7343–7352 (2017).

[43] Roozban N., Abbasi S., Ghazizadeh M., Statistical Analysis of the Photocatalytic Activity of Decorated Multi-Walled Carbon Nanotubes with ZnO Nanoparticles, *Journal of Materials Science Materials in Electronics*, **28(8)**: 6047–6055 (2016).

[44] Jeevanandam J., Chan Y.S., Danquah M.K., Biosynthesis and Characterization of MgO Nanoparticles from Plant Extracts Via Induced Molecular Nucleation, *New J. Chem.*, **41**:2800–2814 (2017).

[45] Mahmoud H.R., Ibrahim S.M., El-Molla S.A., Textile Dye Removal from Aqueous Solutions using Cheap MgO Nanomaterials: Adsorption Kinetics, Isotherm Studies and Thermodynamics, *Adv. Powder Technol*., **27**: 223–231 (2016)

[46] Niu H., Yang Q., Tang K., Xie Y., Large-Scale Synthesis of Single-Crystalline MgO with Bone-Like Nanostructures, *J. Nanoparticle Res*., **8**: 881–888 (2006).

[47] Jadhav A.H., Lim A.C., Thorat G.M., Jadhav H.S., Seo J.G., Green Solvent Ionic Liquids: Structural Directing Pioneers for Microwave-Assisted Synthesis of Controlled MgO Nanostructures. *RSC Adv*., **6**: 31675–31686 (2016).

[48] Heidarizad M., Şengör S.S., Synthesis of Graphene Oxide/Magnesium Oxide Nanocomposites with High-Rate Adsorption of Methylene Blue, *J. Mol. Liq.*, **224**: 607–617(2016).

[49] Jawad A.H., Mubarak N.S.A., Abdulhameed A.S., Tunable Schiff's Base-Cross-Linked Chitosan Composite for the Removal of Reactive Red 120 Dye: Adsorption and Mechanism Study, *Int. J. Biol. Macromol.*, **142**: 732–741 (2020).

[50] Ma J., Zhuang Y., Yu F., adsorption Studies of Organic Pollutants from Aqueous Solution onto CNT/C @ Fe / Chitosan, *New J Chem.* **39**: 9299-9305 (2015).

[51] Srivastava V., Sharma Y.C., Sillanpää M., Green Synthesis of Magnesium Oxide Nanoflower and Its Application for the Removal of Divalent Metallic Species from Synthetic Wastewater, *Ceram Int*., **41**: 6702–6709 (2015).

[52] Yousefi S., Ghasemi B., Tajally M., Asghari A., Optical Properties of MgO and $Mg(OH)_2$ Nanostructures Synthesized by a Chemical Precipitation Method Using Impure Brine, *J. Alloys Compd*., **711**: 521-529 (2017).

[53] Abdulhameed A.S., Mohammad A.K.T., Jawad A.H., Application of Response Surface Methodology for Enhanced Synthesis of Chitosan Tripolyphosphate/ TiO_2 Nanocomposite and Adsorption of Reactive Orange 16 Dye. *J. Clean Prod*., **232**:43–56(2019).

[54] Pooralhossini J., Ghaedi M., Zanjanchi M.A., Asfaram A., Ultrasonically Assisted Removal of Congo Red, Phloxine B and Fast Green FCF in Ternary Mixture Using Novel Nanocomposite Following their Simultaneous Analysis by Derivative Spectrophotometry, *Ultrason Sonochem*., **37**: 452–463 (2017).

[55] Bagheri A.R., Ghaedi M., Asfaram A., Hajati S., Ghaedi A.M., Bazrafshan A.A., Rahimi M.R.,, Modeling and optimization of Simultaneous Removal of Ternary Dyes onto Copper Sulfide Nanoparticles Loaded on Activated Carbon Using Second-Derivative Spectrophotometry, *J. Taiwan Inst. Chem. Eng*., **65**: 212–224 (2016).

[56] Lagergren S., About the Theory of SO-Called Adsorption of soluble Substance, *Kungliga Svenska Vetenskapsakademiens Handlingar*, **24**:1–39 (1898).

[57] Ho Y.S., Mckay G., Pseudo-Second order Model for Sorption Processes, *Process Biochem*, **34**: 451–465 (1999).

[58] Allen J.A., Scaife P.H., The Elovich Equation and Chemisorption Kinetics, *Aust J. Chem*., **19**: 2015-2023 (1966).

[59] Wu F-C, Tseng R-L, Juang R-S., Initial Behavior of Intraparticle Diffusion Model Used in the Description of Adsorption Kinetics, *Chem. Engg Journal*, **153(1–3)**: 1-8(2009)

[60] Langmuir I., The Adsorption of Gases on Plane Surfaces of Glass, Mica and Platinum, *J. Am. Chem. Soc*., **40**: 1361–1403 (1918).

[61] Freundlich H., Über die Adsorption in Lösungen, *Zeitschrift für Phys Chemie* 57U: (1907)

[62] Aharoni C, Ungarish M., Kinetics of Activated Chemisorption-part 2.- Theoretical Models, *J. Chem. Soc. Faraday Trans. 1*, **73**: 456–464(1977)

[63] Redlich O, Peterson DL., A Useful Adsorption Isotherm, *J. Phys. Chem*., **63**:1024–1024(1959).

[64] Tanhaei B., Ayati A., Lahtinen M., Sillanpää M., Preparation and Characterization of a Novel Chitosan/Al_2O_3/Magnetite Nanoparticles Composite Adsorbent for Kinetic, Thermodynamic and Isotherm Studies of Methyl Orange Adsorption, *Chem. Eng. J*., **259**: 1–10 (2015).

[65] Jiang R., Zhu H., Fu Y., Equilibrium and Kinetic Studies on Adsorption of Methyl Orange from Aqueous Solution on Chitosan/Kaolin/γ-Fe_2O_3 Nanocomposite. *Int. Conf Remote Sensing, Environ Transp. Eng. RSETE 2011 - Proc* 7565–7568. (2011).

[66] Attallah O.A., Al-Ghobashy M.A., Nebsen M., Salem M.Y., Removal of Cationic and Anionic Dyes from Aqueous Solution with Magnetite/Pectin and Magnetite/Silica/Pectin Hybrid Nanocomposites: Kinetic, Isotherm and Mechanism Analysis, *RSC Adv.*, **6**: 11461-11480 (2016).

[67] Cho D-W., Jeon B-H., Chon C-M., Schwartz F.W., Jeong Y., Song H., Magnetic Chitosan Composite for Adsorption of Cationic and Anionic Dyes in Aqueous Solution, *J. Ind. Eng. Chem.*, **28**:60-66 (2015).

[68] Zhu H.Y., Jiang R., Xiao L., Zeng G.M., Preparation, Characterization, Adsorption Kinetics and Thermodynamics of Novel Magnetic Chitosan Enwrapping Nanosized γ-Fe_2O_3 and Multi-Walled Carbon Nanotubes with Enhanced Adsorption Properties for Methyl Orange, *Bioresour Technol*., **101**: 5063-5069 (2010).

[69] Zhang J, Zhou Q, Ou L., Kinetic, Isotherm, and Thermodynamic Studies of the Adsorption of Methyl Orange from Aqueous Solution by Chitosan/Alumina Composite, *J. Chem. Eng. Data.*, **57**: 412-419 (2012).